Published in final edited form as:
Neuroscience. 2010 September 1; 169(3): 951–964. doi:10.1016/j.neuroscience.2010.06.005.

Distribution of NBCn2 (SLC4A10) splice variants in mouse brain

Ying Liu[1,2], **Kui Xu**[4], **Li-Ming Chen**[1,2], **Xiaoyan Sun**[1], **Mark D. Parker**[1,3], **Michelle L. Kelly**[3], **Joseph C. LaManna**[1], and **Walter F. Boron**[1,3]

[1]Department of Physiology and Biophysics, Case Western Reserve University School of Medicine, Cleveland, OH 44106, USA

[2]Department of biological sciences, Key Laboratory of Molecular Biophysics of Ministry of Education, Huazhong University of Science & Technology School of Life Science & Technology, Wuhan, Hubei Province 430074, China

[3]Department of Cellular and Molecular physiology, Yale University School of Medicine, New Haven, CT 06520, USA

[4]Department of Neurology, University Hospitals of Cleveland, Cleveland, OH 44106, USA

Abstract

The five known Na-coupled HCO_3^- transporters (NCBTs) of the solute carrier 4 (SLC4) family play important roles in pH regulation and transepithelial HCO_3^- transport. Nearly all of the NCBTs have multiple splice variants. One particular NCBT, the electroneutral Na/HCO_3^- cotransporter NBCn2 (SLC4A10), which is predominantly expressed in brain, has three known splice variants—NBCn2-A, -B, and -C—as well as a potential variant -D. It is important to know the tissue-specific expression of the splice variants for understanding the physiological roles of NBCn2 in central nervous system. In the present study, we developed three novel rabbit polyclonal antibodies against NBCn2: (1) anti-ABCD, which recognizes all four variants; (2) anti-BD, which recognizes NBCn2-B and -D; (3) anti-CD, which recognizes NBCn2-C and -D. By western blotting, we examined the expression and distribution of NBCn2 splice variants in five brain regions: cerebral cortex, subcortex, cerebellum, hippocampus, and medulla. The expression pattern revealed with anti-ABCD is distinct from those revealed with anti-BD and anti-CD. Moreover, by using immunoprecipitation in combination with western blotting, we demonstrate that NBCn2-D does indeed exist and that it is predominantly expressed in subcortex, to a lesser extent in medulla, but at very low levels in cortex, cerebellum, and hippocampus. NBCn2-A may be the dominant variant in mouse brain as a whole, and may also dominate in cerebral cortex, cerebellum, and hippocampus. Immunohistochemistry with anti-ABCD shows that NBCn2 is highly expressed in

Address correspondence to: Walter Boron, Department of Physiology and Biophysics, Case Western Reserve University School of Medicine, 10900 Euclid Ave. Wood Building W-464, Cleveland, OH 44106, Tel: 216-368-3400; FAX: 216-368-3952, walter.boron@case.edu, **Ying Liu**, Department of Biological Sciences, Key Laboratory of Molecular Biophysics of Ministry of Education, Huazhong University of Science & Technology School of Life Science and Technology, 1037 Luoyu Rd. Wuhan, Hubei Province 430074, China, Tel: 86-27-87795906, liuying@mail.hust.edu.cn.

DISCLOSURES

This work was supported by grants R01-NS18400 (to WFB), P01-HD32573 (PI: Gabriel G. Haddad, UCSD), and R01-NS38632 (to JCL). Dr. Michelle L. Kelly was supported by institutional NIH training grant T32-NS07455 (PI: Emile L. Boulpaep, Yale University) and individual NIH postdoctoral fellowship F32-NS053199.

choroid plexus, cortex, molecular layer of cerebellum, hippocampus, and some specific regions of the brainstem.

Keywords

electroneutral bicarbonate transporter; immunohistochemistry; neuron; central nervous system

INTRODUCTION

The five known Na-coupled HCO_3^- transporters (NCBTs)—all members of the solute carrier 4 (SLC4) family—play important roles in the regulation of extra- as well as intracellular pH as well as the transepithelial acid-base transport (for review, see Romero et al., 2004). Among the five NCBTs, two are electrogenic Na/HCO_3 cotransporters (NBCe1, NBCe2), two are electroneutral Na/HCO_3 cotransporters (NBCn1, NBCn2), and a fifth is also electroneutral, the Na-driven Cl-HCO_3 exchanger (NDCBE). The three electroneutral transporters are preferentially expressed in the central nervous system.

NBCn2 (SLC4A10) was first cloned from a mouse insulinoma cell line (Wang et al., 2000), and was originally characterized as a Na^+-driven Cl-HCO_3 exchanger and named NCBE. However, Parker et al. have demonstrated that SLC4A10 is actually an electroneutral Na/HCO_3^- cotransporter under physiological conditions, with Cl self-exchange activity. Thus, they renamed it NBCn2 (Parker et al., 2008b). Jacob et al demonstrated that the knock-out of *slc4a10* is associated with an increased epilepsy threshold in mice (Jacobs et al., 2008). On the other hand, a translocation breakpoint in the human *SLC4A10* gene is associated with partial epilepsy, along with mental retardation, and cognitive impairment (Gurnett et al., 2008).

Two known alternative splicing units—the DNA inserts A and B—exist in the human *SLC4A10* gene and the rodent *slc4a10* gene. Insert A is a 90-bp exon, which encodes a 30-aa cassette within the cytosolic N terminus (Nt), whereas insert B corresponds to an 39-bp exon that encodes 3 aa before a stop codon. Thus, insert B encodes one of two alternative ends of the cytosolic C terminus (Ct). The alternative splicing of these two inserts theoretically could give rise to four splicing variants of NBCn2: NBCn2-A, -B, -C, and -D (Fig. 1; for review, see Parker and Boron, 2007). In 2002, Choi et al. cloned NBCn2-A and NBCn2-B from human brain and kidney (Choi et al., 2002). NBCn2-A is the ortholog to the mouse clone originally identified by Wang et al (Wang et al., 2000). NBCn2-B differs from NBCn2-A by containing insert A, which corresponds to cassette A in the protein. The mRNAs encoding both NBCn2-A and NBCn2-B have the 39-bp insert B, the stop codon of which produces a “short” Ct.

In 2003, Giffard et al. identified two NBCn2 splice variants from rat brain, which they named as rb1NCBE and rb2NCBE (Giffard et al., 2003). rb1NCBE is the ortholog of human NBCn2-B. rb2NCBE corresponds to NBCn2-C, which lacks both inserts A and B. Because of the absence of the stop codon in insert B, NBCn2-C has a unique 21-aa “long” Ct that contains a PDZ-binding motif. Giffard et al. have reported a partial rat clone that corresponds to NBCn2-D (Giffard et al., 2003). A recent study shows that humans can splice out insert B (Parker et al., 2008b), providing the potential to create NBCn2-C and NBCn2-D. An analysis of the genomes of the three aforementioned species—human, rat, and mouse—indicates that all three species could in principle produce all four splice variants of NBCn2.

Using northern blotting (Parker et al., 2008b; Wang et al., 2000) as well as RT-PCR analysis (Damkier and Praetorius, 2007; Parker et al., 2008b), investigators have shown that NBCn2 transcripts are predominantly expressed in brain. It has been demonstrated (Praetorius et al., 2004), and confirmed (Chen et al., 2008b; Jacobs et al., 2008), that NBCn2 is expressed in the basolateral membrane of choroid plexus epithelium. Interestingly, a mouse with *slc4a10* knock-out (KO) has smaller brain ventricles than wild-type. This observation suggests that NBCn2 plays an important role in the production of cerebrospinal fluid (Jacobs et al., 2008). Moreover, Chen et al demonstrated on the protein level that NBCn2 is expressed in cultured as well as freshly dissociated hippocampal neurons, but not in astrocytes (Chen et al., 2008b). An antibody targeting the N-terminal 71–85 aa of NBCn2 stains hippocampal-CA3 pyramidal cells in wild-type mice, but not in mice with a disrupted *slc4a10* gene (Jacobs et al., 2008).

Rat NBCn2-C (rb2NCBE) has a greater functional expression than rat NBCn2-B (rb1NCBE; see Giffard et al., 2003). Immunofluorescence and co-immunoprecipitation studies on transfected cells indicate that NBCn2-C colocalizes with ezrin binding protein 50 (EBP50), a PDZ-domain protein. Also known as NHERF1, EBP50 appears to be a scaffold protein that couples a variety of integral membrane proteins to downstream effectors. Moreover, the inhibition of protein kinase A (PKA) increased NBCn2-C activity. These observations suggest that the regulation of NBCn2-C involves PKA and a multiprotein signaling complex (Lee et al., 2006).

It is important to know the tissue-specific distribution of the NBCn2 splice variants for understanding the physiological roles of NBCn2. In the present study, we developed and characterized three novel rabbit polyclonal antibodies, one against the first 18 aa common to all known splice variants of the human NBCn2 Nt, a second against 18 aa within the 30 residues of cassette A of human NBCn2-B and -D, and a third against the 21 aa of the unique long Ct of NBCn2-C and -D. We tested the specificity of these antibodies by western blotting. Using these antibodies, we examined the expression and distribution of the common Nt as well as the two different NBCn2 cassettes in five brain regions—cerebral cortex, subcortex, cerebellum, hippocampus, and medulla—of the adult mouse. Moreover, we examined the expression of NBCn2 in mouse brain by immunofluorescence.

METHODS

Peptides and antibodies

Table 1 summarizes the peptides—based on human sequences—used to generate the new polyclonal antibodies. The peptides were conjugated to keyhole limpet hemocyanin (KLH) using the Imject Maleimide-Activated mcKLH Kit (Pierce, Rockford, IL, USA) before immunization of the rabbits. The antisera were affinity-purified with the corresponding immunogen peptide, using the CarboxylLink™ Kit (Pierce) following the manufacturer's instructions.

For western blotting with immunoprecipitated samples, affinity-purified primary antibodies (anti-BD or anti-CD) were conjugated to activated-peroxidase, using EZ-Link® Plus Activated Peroxidase Kit (Pierce) following the manufacturer's instructions.

For immunodepletion, the affinity-purified NBCn2-ABCD antibody was diluted in PBS, incubated in a column for 2 hrs with a Pierce CarboxylLink™ gel, and linked with the corresponding immunogenic peptides. The flow-through was then collected, concentrated, and used as a negative control in immunohistochemistry staining.

In addition to the new antibodies, we also used anti-EGFP (Living Colors® A.v. monoclonal antibody JL-8, Catalog# 632381, Clontech, Carlsbad, CA), MAP2 (Cat# MAB3418, Chemicon International, Temecula, CA), anti-AQP1 (1/A5F6; Santa Cruz Biotechnology, Cat. # sc-58610), and an anti-NDCBE described previously (Chen et al., 2008b).

Construction of enhanced green fluorescent protein (EGFP)-tagged NCBTs in Xenopus expression vectors

Constructing hNBCe-1-B-EGFP.pGH19—Our starting material was hNBCe1-B.pGH19 (Choi et al., 1999). In the pGH19 *Xenopus* oocyte expression vector, hNBCe1-B is flanked by the 5′- and 3′-UTRs of *Xenopus* β-globin. We introduced an *Age*I restriction site at a position preceding the termination codon of the NBCe1-B open reading frame (ORF) by Quickchange® Site-Directed Mutagenesis (Stratagene, La Jolla, CA). The mutant construct was restricted using *Age*I and *Xho*I to remove a DNA fragment that contained the termination codon of hNBCe1-B and the 3′-UTR of *Xenopus* β-globin. The excised fragment was replaced by a DNA cassette with the structure *Age*I–EGFP cDNA / *Xenopus* β-globin 3′-UTR–*Xho*I (*Age*I-EGFP-*Xho*I (Chen et al., 2008b). The final construct hNBCe1-B–EGFP.pGH19 contained the ORF of hNBCe1-B, fused in-frame to the EGFP ORF via the 5-aa linker sequence ‘SPVAT’.

Constructing EGFP-hNBCe2-C.pKSM—Our starting material was hNBCe2-C.pKSM—that is, human NBCe2-C cDNA in the pKSM *Xenopus* oocyte expression vector (Virkki et al., 2002), flanked by the 5′- and 3′-UTRs of *Xenopus* β-globin. We introduced an *Age*I restriction site by Stratagene Quickchange® Site-Directed Mutagenesis at a position that is 63 nts upstream of the initiator Met_1 of the hNBCe2-C ORF. The resulting construct was restricted using *Age*I and *Kpn*I (*Kpn*I cuts at a recognition sequence 56 nts upstream of Met_1) to produce an “acceptor” construct *Kpn*I–hNBCe2-C–pKSM–*Age*I. A 700-bp “donor” insert fragment *Age*I–*EG*FP–*Kpn*I, without a termination codon, was amplified from NBCe1-A–EGFP.pGH19 (Toye et al., 2006), digested with *AgeI* and *KpnI* and ligated into the acceptor vector. The resulting construct— EGFP-hNBCe2-C.pKSM—contained the ORF of EGFP, fused in-frame to the hNBCe2-C ORF via the 21-aa linker sequence ‘GYHLFFLQKLRINAQLWAPRV’.

Constructing NBCn2-D–EGFP.pGH19—Our starting material was hNBCn2-B–EGFP.pGH19 (NCBE-EGFP in (Chen et al., 2008b). That is, the pGH19 *Xenopus* expression vector containing cDNA encoding human NBCn2-B fused in-frame with EGFP via the 6 aa linker sequence ′CSPVAT’. In order to create an NBCn2-D version of this construct, it was necessary to remove the 9 nt sequence ′TCCCCTTCC′ that encodes the unique 3 aa Ct of NBCn2-B (amino acids ′SPS′) and replace them with the 63 nt sequence ′ATTGAAAGCCGAAAAGAGAAGAAAGCTGACTCAGGGAAAGGTGTTGACAGGG AGA CTTGTCTA′ that encodes the unique 21-aa Ct of NBCn2-D (amino acids ′IESRKEKKADSGKGVDRETCL′). This conversion of NBCn2-B–EGFP to NBCn2-D–EGFP was effected in six rounds of Stratagene Quick-Change® site-directed mutagenesis performed according to the manufacturer’s recommendations.

Previously described were the construction of rNBCn1-B-EGFP.pGH19 (Chen et al., 2008b) and hNDCBE-B.pGH19 (Grichtchenko et al., 2001).

cRNA injection of oocytes

Xenopus ovarian lobes were purchased from Nasco (Fort Atkinson, WI, USA). Oocytes were separated by collagenase digestion as previously described (Chen et al., 2008b). Stage of V–VI oocytes were selected and kept at 18 °C in OR3 medium until use.

cDNA constructs were linearized by NotI digestion. Capped cRNA was synthesized by using T7 or T3 mMessage mMachine kit (Ambion, Austin, TX) with linearized cDNA in pGH19 or pKSM as templates. 50 nl cRNA of 0.5 μg/μl was injected to oocyte. Oocytes were kept in OR3 medium for 4 to 5 days until use.

Preparation of membrane proteins and western blotting

Tissues were collected from C57/BL mice, which were housed according to protocols approved by the Animal Care and Use Committee at Case Western Reserve University. Membrane proteins either from brain tissues of 2-month-old, adult mice or from oocytes were prepared as previously described (Chen et al., 2008b) with slight modifications. In the present paper, we define five rather than four brain regions—dividing the previously defined subcortex into subcortex (including basal ganglia, thalamus, hypothalamus, and structures caudad up to and including the pons) and medulla. Tissues of cerebral cortex, subcortex, cerebellum, hippocampus, and medulla were dissected. Total protein concentration was measured with the BCA Protein Assay Kit (Pierce). Membrane proteins were mixed with 2× SDS-sample buffer containing 6 M urea, and were denatured at 95°C. The proteins were separated on 4–20 % Tris-HCl ready gels (Bio-Rad, Hercules, CA, USA) and then transferred to Immobilon™ PVDF membranes (Millipore, Bedford, MA). The blots were blocked with 5% milk, incubated with crude antiserum or affinity-purified antibodies in 1% milk in TBST at room temperature (RT) for 1 hr, washed with TBST, and then incubated with secondary antibody for 1 hr at RT. After washing the membrane with TBST, we performed chemiluminescence with Amersham™ ECL plus western-blotting detection system (GE Healthcare, Buckinghamshire, UK) prior to X-ray film exposure. Western blots were scanned with an Epson V500 photo scanner. Densitometry of bands corresponding to NBCn2 were measured with ImageJ (an open-source Java imageprocessing software inspired by NIH. http://rsb.info.nih.gov/ij/).

Immunoprecipitation

100 μg mouse-brain membrane proteins were diluted in 1.2 ml TENT buffer (50 mM This-HCl, 5 mM EDTA, 150 mM NaCl, 5% Triton X-100, pH7.5) containing 1% protease inhibitor cocktail for mammalian tissues (Sigma-Aldrich). 5 μl crude antiserum of either the anti-BD antibody or the anti-CD antibody, together with 25 μl of a 50% suspension of CALBIOCHEM® protein G plus A-agarose beads (EMD, Darmstadt, Germany), were added. The immunoprecipitation tubes were rotated overnight at 4 °C. The next day, the beads were washed for 3 times with 1 ml TENT buffer, and washed twice with 1 ml NET2 buffer (10 mM this-HCl, 2 mM EDTA, 0.1% SDS, pH7.5). Beads were suspended with 40 μl 1X SDS loading buffer containing 3M urea, and then heated at 95°C for 3 minutes. Samples were separated with beads by spinning through micro-spin® columns (Pierce). Equal amounts of samples were loaded onto two 4–20 % Tris-HCl ready gels (Bio-Rad), followed by western blotting with either HRP-conjugated anti-BD antibody or HRP-conjugated anti-CD antibody at the desired dilution.

Histology and immunohistochemistry

A two-month old, adult mouse was transcardially perfused and fixed with 4% paraformaldehyde in phosphate buffer (pH 7.4). The brain was removed and immersion-fixed overnight in 4% paraformaldehyde at 4 °C. The tissues were embedded in Tissue-Tek® OCT medium, and then serial sagittal sections (5 μm) were made. For histological examination, sections were stained with thionin and viewed under a light microscope. For immunohistochemistry, sections were rehydrated with TBS (10 mM Tris-HCl, 150 mM NaCl, pH7.4). To enhance permeability, slides were soaked in 1% SDS in TBS for 15 min, followed by 6-min washes ×5 with TBST. Endogenous peroxidase activity was blocked by 0.3% H_2O_2 in TBS. After we washed the slides with TBST, we blocked with 5% normal

goat serum (NGS) in TBS ×30 min. Then the slides were incubated with affinity-purified anti-ABCD antibody or immunodepleted anti-ABCD antibody at 1:1000 dilution, together with a mouse monoclonal anti-MAP2 at 1:100 dilution or a mouse monoclonal anti-AQP1 at 1:200 dilution in TBS containing 2.5% NGS and 0.025% Triton X-100 for 1 hr at RT. After the wash with TBST, we incubated the slides with HRP-conjugated goat-anti-rabbit secondary antibody (Vector laboratories, Burlingame, CA, USA) at 1:200 dilution and Cy2-goat anti-mouse secondary antibody (Jackson immunoResearch Laboratories, Inc., West Grove, PA, USA) at 1:100 dilution in TBS containing 2.5% NGS and 0.025% Triton X-100 for 1 hr at RT. After the wash, slides were treated with signal amplification reagent TSA™ plus Tetramethylrhodamine System (at 1:100 dilution; PerkinElmer Life Sciences) according to the manufacturer's instructions.

Statistics analysis

To compare the distribution of NBCn2 variants in different mouse-brain sections, oneway ANOVA in combination with Student-Newman-Keuls (SNK) multiple comparison was performed, using KaleidaGraph (version 4, Synergy Software). $P<0.05$ was considered significant.

RESULTS

Validation of the polyclonal antibodies

We first examined the specificity of our novel NBCn2 polyclonal antibodies by western blotting with membrane proteins from oocytes injected with H_2O or oocytes expressing full-length hNBCe1-B-EGFP, EGFP-hNBCe2-C, rNBCn1-B-EGFP, hNBCn2-B-EGFP, hNBCn2-D-EGFP, hNDCBE-B. Fig. 2A shows that anti-ABCD specifically recognizes NBCn2, but not full-length NBCe1, NBCe2, NBCn1, or NDCBE. Fig. 2B shows anti-BD specifically recognizes NBCn2-B, but not NBCe1, NBCe2, NBCn1, or NDCBE. Anti-CD specifically recognizes NBCn2-D, but not NBCe1, NBCe2, NBCn1, NBCn2-B, or NDCBE (Fig. 2C). In all cases, the novel antibodies reveal two bands for EGFP-tagged NBCn2 (lane 5 in Fig. 2A, lane 5 in Fig. 2B and lane 6 in Fig. 2C). The lower bands at a molecular weight (MW) of ~ 150 kDa presumably represent the slightly glycosylated forms of NBCn2 (Chen et al., 2008b); the predicted MW for hNBCn2-B-EGFP is 153.9 kDa, and the predicted MW for hNBCn2-D-EGFP is 156.2 kDa. The upper bands presumably represent the highly N-glycosylated forms of NBcn2 (Chen et al., 2008b).

By reprobing the blots with anti-EGFP antibody, we confirmed the expression of the three negative controls: hNBCe1-B-EGFP, EGFP-hNBCe2-C, and rNBCn1-B-EGFP as well as hNBCn2-B-EGFP and hNBCn2-D-EGFP (data not shown). We also confirmed (data not shown) the expression of the negative control hNDCBE-B by using anti-NDCBE described previously (Chen et al., 2008a).

Expression of NBCn2 variants in mouse brain

We examined the expression of NBCn2 in five regions of mouse brain: cerebral cortex, subcortex, cerebellum, hippocampus, and medulla. As shown in Fig. 3A, C, and E, all three antibodies reveal a band at MW of ~150 kDa, which presumably represents the highly glycosylated form of NBCn2 (Chen et al., 2008b).

Fig. 3A shows a typical blot probed with anti-ABCD, which recognizes all four NBCn2 variants, and thus reveals the distribution of the sum of all NBCn2 variants. Fig. 3B summarizes the mean densitometry from six experiments, such as the one shown in Fig. 3A.

Fig. 3C shows a typical blot probed with anti-BD, which recognizes NBCn2-B and -D, and thus reveals the distribution of NBCn2-B/D. Fig. 3D summarizes the mean densitometry from six experiments, such as that shown in Fig. 3C.

Finally, Fig. 3E shows a typical blot probed with anti-CD, which recognizes NBCn2-C and -D, and thus reveals the distribution of NBCn2-C/D. Fig. 3F summarizes the mean densitometry from six experiments, such as the one shown in Fig. 3E.

From the bar graphs, we can see that both anti-BD and anti-CD reveal patterns that are different from that of anti-ABCD. The patterns for anti-BD and anti-CD are similar except that the anti-CD signal is particularly high in cerebellum. Thus, different NBCn2 variants must have different tissue distributions.

Immunoprecipitation

We examined the relative distribution of NBCn2-D using a combination of immunoprecipitation and western blotting. In principal, by immunoprecipitating with anti-BD and probing with anti-CD, or vice versus, we can obtain the distribution of NBCn2-D. The upper half of Fig. 4A shows an experiment in which we immunoprecipitated NBCn2 from membrane proteins of mouse brain using anti-BD, and then probed the blot with the same antibody (anti-BD). The lower half of Fig. 4A summarizes the mean densitometric data of four such experiments. The distribution pattern in the lower half of Fig. 4A is similar to that in Fig. 3D.

The upper half of Fig. 4B shows a blot parallel to the one shown in Fig. 4A (i.e., immunoprecipitated with anti-BD), but probed with anti-CD. Because the only commonality between the two antibodies is ‘D’, the mean densitometric data (lower half of Fig. 4B) represents the relative distribution of NBCn2-D.

The two lower panels of Fig. 4 show the results from experiments in which we immunoprecipitated NBCn2 with anti-CD and then probed the blots with anti-CD (Fig. 4C) or anti-BD (Fig. 4D). Not surprisingly, the lower half of Fig. 4C (representing the distribution of NBCn2-CD) shows a pattern similar to that in Fig. 3F. The upper and lower halves of Fig. 4D (representing the distribution of NBCn2-D) show patterns that are virtually identical to their counterparts in Fig. 4B. Considering Fig. 4B and D together, we conclude that: (1) NBCn2-D exists. And (2) NBCn2-D is predominantly expressed in subcortex and to a somewhat lesser extent in medulla, but—relative to subcortex and medulla—is expressed at much lower levels in cortex, cerebellum, and hippocampus.

Immunohistochemistry of NBCn2 in brain sections

To study the tissue and cellular distribution of NBCn2 in mouse brain, we performed immunohistochemistry on mouse brain sections using anti-ABCD, which recognizes all four splice variants of NBCn2. Anti-CD did not work well for immunohistochemistry. Anti-BD worked well, but produced results qualitatively similar to those for anti-ABCD.

In the experiment shown in Fig. 5, we double-stained a section of choroid plexus from the fourth ventricle of mouse brain with affinity-purified anti-ABCD antibody (red in Fig. 5A) and anti-AQP1 antibody (green in Fig. 5B), which is an apical marker for the choroid plexus epithelial cell (Praetorius and Nielsen, 2006). The merged image in Fig. 5C shows that our anti-ABCD antibody specifically stains the basolateral membrane of the epithelial cells of choroid plexus. The thionin-stained section in Fig. 5D provides a histological reference for the immunohistochemistry. Our results for NBCn2 localization in choroid plexus are consistent with previously reported observations (Chen et al., 2008b;Praetorius et al., 2004),

showing that our novel NBCn2 antibody anti-ABCD is specific and reliable for immunohistochemistry.

In sections of cerebrum, double stained with anti-ABCD (red) and the neuronal marker anti-MAP2 (green), NBCn2 is expressed at high levels throughout the cortex (Fig. 6A–C, D–F), at lower levels in striatum (Fig. 6D–F), but is not detectable in corpus callosum (Fig. 6D–F). As shown in a higher-magnification view (Fig. 6G–I), anti-ABCD was positive at or near the plasma membrane of the soma of some neurons (arrows), and especially labeled the processes of neurons (arrow heads).

Fig. 7 shows a section of mouse cerebellum, double stained with anti-ABCD (red) and anti-MAP2 (green). A lower-magnification view (Fig. 7A–C) shows that NBCn2 is expressed at high levels in the molecular layer, but at very low levels in the granular layer. NBCn2 is not detectable in white matter. As shown in a higher-magnification view (Fig. 7D–F), anti-ABCD also stains the cytoplasm of Purkinje cells. In the molecular layer, anti-ABCD labels structures at or near the plasma membrane of some cell soma (arrows) as well as neuronal processes (arrow heads). The NBCn2 signal was absent when the primary anti-ABCD antibody was immunodepleted prior to staining (Fig. 7G–I).

Fig. 8 shows the expression pattern of NBCn2 in the hippocampus, stained with anti-ABCD. NBCn2 is expressed in higher level in dentate gyrus (DG) than in CA1–CA3. The inset shows a thionin-stained section.

Fig. 9A–L show high-magnification views of CA1, CA2, CA3, and DG of hippocampus, double stained with anti-ABCD and anti-MAP2. In each part of the hippocampus, anti-ABCD stains structures at or near the plasma membrane of some pyramidal neurons and granule cells in DG (arrows). However, the staining is strongest in neuronal processes (arrow heads), some of which appear to extend over some neuronal soma (e.g., in DG).

In the brainstem, NBCn2 expression, detected with anti-ABCD, is nonuniform, as shown in a low magnification sagittal view of a portion of the brainstem (Fig. 10A). Low-power views of adjacent thionin-stained sections (not shown) confirmed the identification of specific nuclei. Fig. 10B and C show higher-power views of thionin-stained sections of the lateral superior olive (LSO) and facial nucleus, respectively. Fig. 11 shows sections of these two nuclei, double stained with anti-ABCD and anti-MAP2. NBCn2 generally expresses at very low levels in the facial nucleus (Fig. 11A–C) and lateral superior olive (Fig. 11D–F), but at higher levels in the surrounding area (arrow heads in Fig. 11A and D). However, in the area enclosed by the rectangle in Fig. 11D, NBCn2 is highly expressed in some neurons near the center of the LSO. The high-power view in Fig. 11G–I shows that the NBCn2 is present mostly in the plasma membrane and processes of these neurons.

DISCUSSION

Specificity of the antibodies

The deduced amino-acid sequences of the five known NCBTs are 47% or more identical, and those of the three electroneutral NCBTs are 73% or more identical (for review, see Parker and Boron, 2007). In a previous study, Chen et al developed a polyclonal antibody against the first 135 aa of NBCn2 Nt. The authors suggested that the real epitope could be in the first 18 aa or some short stretches farther downstream (Chen et al., 2008b). In the present study, we developed three novel NBCn2 polyclonal antibodies—directed against the Nt of NBCn2, or Cassette A of NBCn2-B and -D, or the unique Ct of NBCn2-C and -D—and validated their specificities by western-blot analysis of membrane proteins from oocytes expressing different full-length NCBTs. Our data demonstrate that all three antibodies are

specific for NBCn2 or the corresponding NBCn2 variants (Fig. 2) and did not cross react with other members of NCBTs.

Existence of NBCn2-D protein in mouse brain

In mammals, the *slc4a10* gene contains two alternative splicing units: cassette A and B. In principal, *slc4a10* could produce four splice variants of NBCn2. Full-length cDNAs encoding NBCn2-A (Choi et al., 2002; Wang et al., 2000), -B (Giffard et al., 2003; Wang et al., 2000), and -C (Giffard et al., 2003; Wang et al., 2000) have been successfully cloned. Giffard et al. reported a partial clone from rat containing cassette A and lacking cassette B (Giffard et al., 2003). This partial clone presumably corresponds to NBCn2-D shown in Fig. 1. However, to our knowledge, neither the cloning of full-length cDNA nor the demonstration of protein expression has been reported for NBCn2-D. In the present study, we used the combination of immunoprecipitation with anti-BD and then western blotting with anti-CD (Fig. 4A–B), or vice versa (Fig. 4C–D), to investigate the existence of NBCn2-D protein in mouse brain. We detected a band of appropriate molecular weight (Fig. 4B and D), thus demonstrating for the first time—at the protein level—the existence of a fourth splice variant of NBCn2, which is very likely to be “NBCn2-D” as shown in Fig. 1. A complete description will require the cloning of a full-length cDNA encoding NBCn2-D.

Regional distribution of NBCn2 splice variants in mouse brain

In 2003, Giffard et al.—using in situ hybridization with probes within or spanning insert A or B—found that NBCn2 is highly expressed in cortical layers, hippocampus, cerebellum and olfactory bulb in rat brain. However, they found no striking regional differences between probes. Chen et al—employing western-blot analysis and a polyclonal antibody against the first 135 aa of NBCn2—found that total NBCn2 is expressed more in cortex, cerebellum and hippocampus, and less in subcortex (Chen et al., 2008b).

With the development of anti-BD and anti-CD, we are now able, for the first time, to begin to investigate the protein expression of NBCn2 splicing variants in neurons of specific brain regions. The first step of the present study was to test our new anti-ABCD antibody in mouse brain by western blotting. Our results (Fig. 3A) confirm that total NBCn2 is most abundant in cerebellum, cortex and hippocampus, consistent with previous observations (Chen et al., 2008b;Giffard et al., 2003). In addition, we found that the fraction in total NBCn2 proteins is very low in medulla.

Technically, it would be extremely difficult if not impossible to develop single antibodies to indentify individual splicing variants of NBCn2. A major goal of the present study was to glean some insight into the distribution of certain NBCn2 splice variants in mouse brain using a combination of anti-BD and anti-CD antibodies. By western blotting with anti-BD, we found the distribution pattern of NBCn2-B/D (Fig. 3C, D) is distinct from that of the total NBCn2 protein as revealed with anti-ABCD (Fig. 3A, B). Similarly, the distribution pattern of NBCn2-C/D (Fig. 3E, F) is distinct from that of total NBCn2 (Fig. 3A, B). Moreover, the distributions of NBCn2-B/D and NBCn2-C/D differ from each other, with NBCn2-C/D having a higher relative distribution in the cerebellum.

Regional distribution of NBCn2-D—By a combination of immunoprecipitation and western blotting with anti-BD and anti-CD antibody, we were able to isolate NBCn2-D, finding that about half is expressed in subcortex and another one-third in medulla. Thus, relatively little NBCn2-D is expressed in cortex, cerebellum or hippocampus (Fig. 4B, D). It is particularly satisfying that the relative distribution of NBCn2-D were very similar whether we immunoprecipitated with anti-BD and blotted with anti-CD (Fig. 4B), or vice versa (Fig. 4D).

Estimation of regional distribution of NBCn2-B and NBCn2-C—Given the information for the distributions of total NBCn2, NBCn2-B/D, NBCn2-C/D, and NBCn2-D, we might speculate on the distributions of NBCn2-B and NBCn2-C. For example, one might imagine that NBCn2-D represents a high fraction of the NBCn2-B/D in SCX and MD of Fig. 4A, as well as of NBCn2-C/D in SCX and MD in Fig. 4C. If this is true, then we might infer that the expression of NBCn2-B and NBCn2-C are both relatively high in CX, CB, and HC, but relatively low in SCX.

Estimation of regional distribution of NBCn2-A—Based upon the data shown in Fig. 3B, D, and F, we can estimate the fractional distribution of NBCn2-A in different mouse brain regions. Let us consider Fig. 3B (here each bar represents the total amount of NBCn2, namely NBCn2-A + -B + -C + -D) and Fig. 3D (here each bar represents the sum of NBCn2-B + -D), and let us assume that all NBCn2 expressed in the MD of Fig. 3B is NBCn2-B/D (i.e., no NBCn2-A or -C are present). In Fig. 12A, we have replotted Fig. 3B. In Fig. 12B, we have rescaled Fig. 3D so that the height of the MD bar in Fig. 12B is the same as the MD bar in Fig. 12A. Thus, the bars in Fig. 12B are estimates of the relative contribution of NBCn2-B/D to total NBCn2 in Fig. 12A. The differences between the corresponding bars in Fig. 12A and Fig. 12B represent the relative amount of NBCn2-A/C in each brain region.

Next, let us consider Fig. 3B and Fig. 3F and assume that all NBCn2 expressed in the MD of Fig. 3B (i.e., Fig. 12A) is NBCn2-C/D (i.e., no NBCn2-A or -B are present). In Fig. 12C, we have rescaled Fig. 3F so that the height of the MD bar in Fig. 12C is the same as the MD bar in Fig. 12A. Thus, the bars in Fig. 12C are estimates of the relative contribution of NBCn2-C/D to total NBCn2 in Fig. 12A. The differences between the corresponding bars in Fig. 12A and Fig. 12C represent the relative amount of NBCn2-A/B in each brain region.

In Table 2, the first data row summarizes the fractional distribution (in %) of total NBCn2 (i.e., A/B/C/D) in various mouse-brain regions, as shown in Fig. 12A. The second row shows our estimates for NBCn2-B/D based upon the above assumptions (as shown in Fig. 12B), and the third row shows our estimates for NBCn2-C/D (as shown in Fig. 12C). By subtracting the values in the second and third rows from the values in the first row, we arrive at the figures in the fourth row. Note that we subtract the contribution of NBCn2-D twice, thus, at least 19% of all the NBCn2 in the mouse brain is NBCn2-A in the CX. Similarly, at least 6% of all NBCn2 is NBCn2-A in the SCX, and so on. View differently, at least 76% (19/25=76%) of all NBCn2 in the CX is NBCn2-A, 35% (6/17=35%) of all NBCn2 in the SCX is NBCn2-A, 68% (21/31=68%) of all NBCn2 in CB is NBCn2-A, and 71% (15/21=71%) of all NBCn2 in HC is NBCn2-A. Of course, because of our initial assumptions (i.e., all NBCn2 in MD is NBCn2-B/D or NBCn2-C/D) and our double subtraction of NBCn2-D, the analysis is not perfect. Thus, it is not surprising that our estimate of NBCn2-A in MD is negative.

Based upon our above analysis, we can infer that NBCn2-A is likely the dominant NBCn2 splice variant expressed in the mouse brain, accounting for half or more of the total NBCn2 protein in brain. Furthermore, we infer that NBCn2-A is the dominant splice variant in CX, CB, and HC. We have already inferred that NBCn2-B and NBCn2-C are likely to be highest in these same three brain regions (i.e., CX, CB, and HC); however, they must be less abundant than NBCn2-A in these same three regions. Finally, the great majority of NBCn2-D is in SCX plus MD, and it is likely that NBCn2-D is the dominant variant in MD. Thus, it appears that each NBCn2 splice variant has a characteristic expression pattern in the mouse central nervous system.

Cellular localization of NBCn2 protein in mouse brain

By immunohistochemistry with mouse cerebral sections, we demonstrate that NBCn2 is highly expressed in cerebral cortex, less in striatum, and not detectable in corpus callosum (Fig.6A). In hippocampus, we find that NBCn2 is expressed in dentate gyrus and CA1–3 (Fig. 8), in general agreement with the expression profile obtained with an antibody against the residues 71–85 of the Nt of NBCn2 (Jacobs et al., 2008). Higher magnification views (Fig. 9) reveal that NBCn2 is expressed in plasma membrane and processes of pyramidal neurons in hippocampus.

In cerebellum, immunohistochemistry with anti-ABCD shows that NBCn2 is abundantly expressed in the molecular layer and Purkinje cells, much less in the granular layer, and not detectable in white matter (Fig. 7A and D). Jacobs et al demonstrated that NBCn2 is highly expressed in cerebellar Purkinje cells and some neocortical interneurons, but not in interneurons in the molecular layer (Jacobs et al., 2008).

Interestingly, our immunofluorescence staining reveals a non-uniform pattern of NBCn2 in brainstem (Fig. 10). In the facial nucleus (Fig. 11A), NBCn2 is expressed very little. In lateral superior olive, NBCn2 is expressed only in particular neurons (Fig. 11D–I).

Possible physiological relevance of NBCn2 splice variants

We are aware of no data that specifically address the physiological role of cassette A or the alternative Ct of NBCn2. As noted in the Introduction, the PDZ-binding motif of NBCn2-C/D is likely responsible for an interaction with EBP50—and possibly with other PDZ proteins—which could impact NBCn2 activity. In NDCBE, which is closely related to NBCn2, an alternative Ct contains an autoinhibitory domain (Parker et al., 2008a). In the case of NBCn1, another close relative of NBCn2, a cassette in the Nt appears to bind the protein phosphatase calcineurin Aβ (Parker and Boron, 2008). Moreover, Cooper et al found that the cassette II of NBCn1 is inhibitory to the functional expression the transporter (Cooper et al., 2006). Thus, it is likely that the splice variants of NBCn2 have an impact on NBCn2 function and thus pHi regulation.

Summary and Conclusions

We generated three novel polyclonal antibodies, one against the extreme Nt of NBCn2, another specific for Cassette A of NBCn2-B/D, and a third specific for the unique C terminus of NBCn2-C/D. Using these antibodies, we studied the relative distribution of NBCn2 splicing variants in mouse brain, and suggest that each of the four NBCn2 splice variants has a characteristic distribution in mouse brain. In addition, we found that NBCn2 is highly expressed in particular neurons in some brainstem nuclei. We hypothesize that the differential distributions of NBCn2 splice variants may reflect regional differences in neuronal acid-base homeostasis.

References

Chen LM, Kelly ML, Parker MD, Bouyer P, Gill HS, Felie JM, Davis BA, Boron WF. Expression and localization of Na-driven Cl-HCO3- exchanger (SLC4A8) in rodent CNS. Neuroscience 2008a; 153:162–174. [PubMed: 18359573]

Chen LM, Kelly ML, Rojas JD, Parker MD, Gill HS, Davis BA, Boron WF. Use of a new polyclonal antibody to study the distribution and glycosylation of the sodium-coupled bicarbonate transporter NCBE in rodent brain. Neuroscience 2008b;151:374–385. [PubMed: 18061361]

Choi I, Rojas JD, Kobayashi C, Boron WF. Functional characterization of "NCBE", an electroneutral Na/HCO3 cotransporter. FASEB J 2002;16:A796.

Choi I, Romero MF, Khandoudi N, Bril A, Boron WF. Cloning and characterization of a human electrogenic Na^+-HCO_3^- cotransporter isoform (hhNBC). Am J Physiol 1999;276:C576–C584. [PubMed: 10069984]

Cooper DS, Lee HJ, Yang HS, Kippen J, Yun CC, Choi I. The electroneutral sodium/bicarbonate cotransporter containing an amino terminal 123-amino-acid cassette is expressed predominantly in the heart. J Biomed Sci 2006;13:593–595. [PubMed: 16547769]

Damkier HH, Praetorius J. Expression of sodium dependent HCO_3^- transporters in human tissues. FASEB J 2007;21:A1284.

Giffard RG, Lee YS, Ouyang YB, Murphy SL, Monyer H. Two variants of the rat brain sodium-driven chloride bicarbonate exchanger (NCBE): developmental expression and addition of a PDZ motif. Eur J Neurosci 2003;18:2935–2945. [PubMed: 14656289]

Grichtchenko II, Choi I, Zhong X, Bray-Ward P, Russell JM, Boron WF. Cloning, characterization, and chromosomal mapping of a human electroneutral Na^+-driven Cl-HCO3 exchanger. J Biol Chem 2001;276:8358–8363. [PubMed: 11133997]

Gurnett CA, Veile R, Zempel J, Blackburn L, Lovett M, Bowcock A. Disruption of Sodium Bicarbonate Transporter SLC4A10 in a Patient With Complex Partial Epilepsy and Mental Retardation. Arch Neurol 2008;65:550–553. [PubMed: 18413482]

Jacobs S, Ruusuvuori E, Sipila ST, Haapanen A, Damkier HH, Kurth I, Hentschke M, Schweizer M, Rudhard Y, Laatikainen LM, Tyynela J, Praetorius J, Voipio J, Hubner CA. Mice with targeted Slc4a10 gene disruption have small brain ventricles and show reduced neuronal excitability. Proc Natl Acad Sci U S A 2008;105:311–316. [PubMed: 18165320]

Lee YS, Ouyang YB, Giffard RG. Regulation of the rat brain Na^+ -driven Cl/HCO_3^- exchanger involves protein kinase A and a multiprotein signaling complex. FEBS Lett 2006;580:4865–4871. [PubMed: 16916513]

Parker, MD.; Boron, WF. Seldin and Giebisch's The Kidney: Physiology and Pathophysiology. Alpern, RJ.; Hebert, SC., editors. Burlington, MA: Academic Press; 2007. p. 1481-1497.

Parker MD, Boron WF. Splice cassette II within the N terminus of the electroneutral Na+ coupled bicarbonate transporter NBCn1 includes a functional calcineurin Aβ binding site. FASEB J 2008;22 759.12.

Parker MD, Bouyer P, Daly CM, Boron WF. Cloning and characterization of novel human *SLC4A8* gene products encoding Na^+-driven Cl-HCO_3 exchanger variants -A, -C and -D. Physiol Genomics 2008a;34:265–276. [PubMed: 18577713]

Parker MD, Musa-Aziz R, Rojas JD, Choi I, Daly CM, Boron WF. Characterization of human SLC4A10 as an electroneutral Na/HCO3 cotransporter (NBCn2) with Cl self-exchange activity. J Biol Chem 2008b;283:12777–12788. [PubMed: 18319254]

Praetorius J, Nejsum LN, Nielsen S. A SCL4A10 gene product maps selectively to the basolateral plasma membrane of choroid plexus epithelial cells. Am J Physiol Cell Physiol 2004;286:C601–C610. [PubMed: 14592810]

Praetorius J, Nielsen S. Distribution of sodium transporters and aquaporin-1 in the human choroid plexus. Am J Physiol Cell Physiol 2006;291:C59–C67. [PubMed: 16481371]

Romero MF, Fulton CM, Boron WF. The SLC4 family of HCO_3 transporters. Pflügers Arch 2004;447:495–509.

Toye AM, Parker MD, Daly CM, Lu J, Virkki LV, Pelletier MF, Boron WF. The human NBCe1-A mutant R881C, associated with proximal renal tubular acidosis, retains function but is mistargeted in polarized renal epithelia. Am J Physiol Cell Physiol 2006;291:C788–C801. [PubMed: 16707554]

Virkki LV, Wilson DA, Vaughan-Jones RD, Boron WF. Functional characterization of human NBC4 as an electrogenic Na^+-HCO_3^- cotransporter (NBCe2). Am J Physiol Cell Physiol 2002;282:C1278–C1289. [PubMed: 11997242]

Wang CZ, Yano H, Nagashima K, Seino S. The Na^+-driven Cl/HCO_3^- exchanger: Cloning, tissue distribution, and functional characterization. J Biol Chem 2000;275:35486–35490. [PubMed: 10993873]

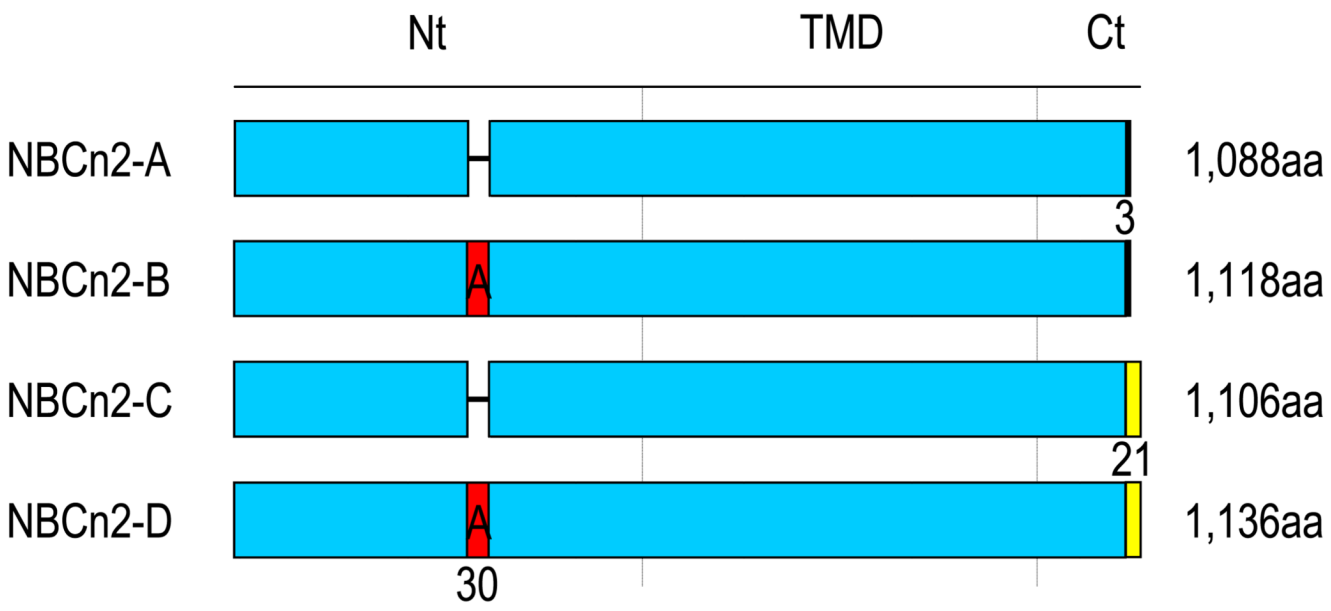

Fig. 1.

Diagram of NBCn2 splice variants. Alignments are based on a combination of protein sequences and genomic analysis. Full-length protein sequences are known for: [1] mouse (m) NBCn2-A (accession # NP_291030) and human (h) NBCn2-A (accession# NP_071341). [2] hNBCn2-B (accession# AAQ83632) and rat (r) rNBCn2-B (aka rb1NCBE; Accession # AAO59640). [3] rNBCn2-C (aka, rb2NCBE, accession# AAO59639). In addition, a partial clone is reported, but no sequence available, for rNBCn2-D (Giffard et al., 2003). The genomic sequences for human (contig span NC_00002.10), rat (contig span NC_000068.6), and mouse (contig span NT_005102.2) each predict a 90-bp exon that corresponds to cassette A (human exon # 11, rat exon # 9, mouse exon # 11), and a 39-bp exon that corresponds to cassette B (human exon # 29, rat exon # 28, mouse exon # 29). Nt: N terminus, TMD: transmembrane domain, Ct: C terminus. Numbers of amino-acid (aa) residues of full-length splice variants are indicated at right. At carboxyl termini, the extreme 3 amino-acid residues of NBCn2-A and -B are different from the extreme 21 aa of NBCn2-C and -D. NBCn2-B and -D contain cassette A of 30 aa. The amino acid numbers of the full length variants refer to the human NBCn2 clones.

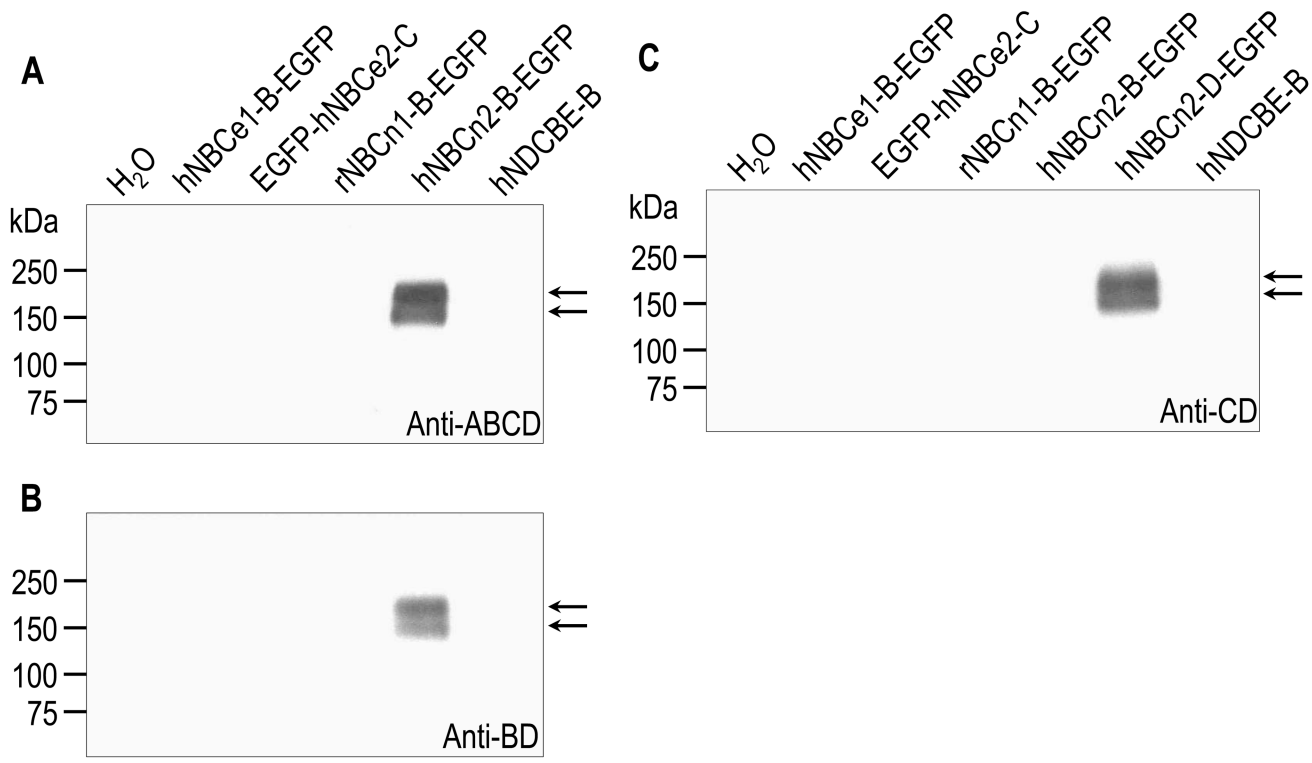

Fig. 2.

Western blotting of membrane proteins from *Xenopus* oocytes expressing different full-length NCBTs. The blots were probed with crude antiserum of anti-ABCD (at 1:2000 dilution, panel A), or crude antiserum of anti-BD (1:1000 dilution, panel B), or affinity-purified anti-CD (1:3000 dilution, panel C). The arrows indicate two bands, presumably representing slightly and highly N-glycosylated forms of NBCn2.

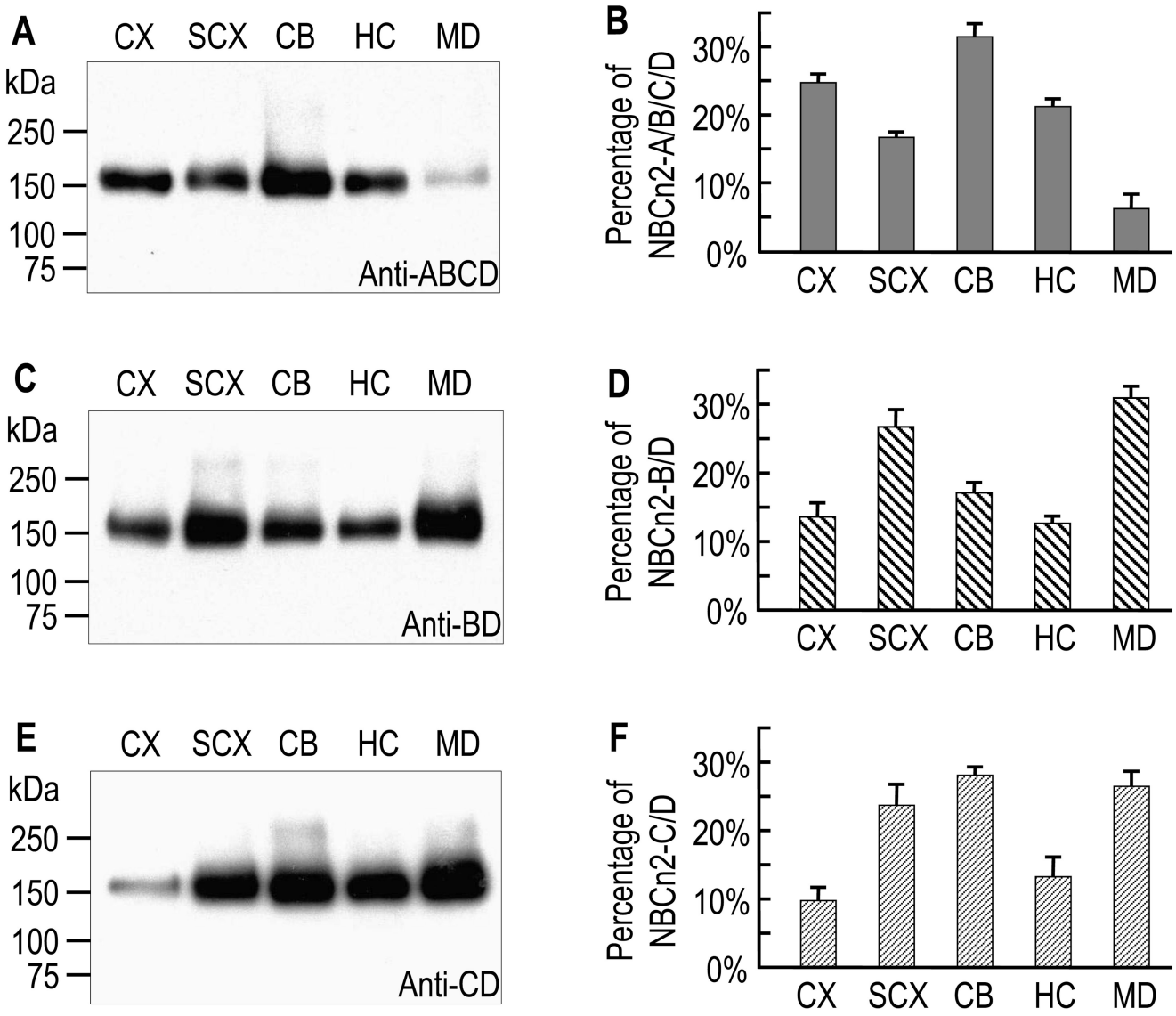

Fig. 3.

Relative distribution of NBCn2 splicing variants in mouse brain regions. (A) Representative western blot of total NBCn2 revealed with anti-ABCD. (B) Relative distribution of total NBCn2. Each western blot was scanned and quantified to obtain densitometry data. For each blot, we summed the total densities of the five brain regions, and then expressed the density of each region as a fraction of 100%. The bar graph represents mean values from 6 blots like that shown in panel A. (C) Typical western blot of NBCn2-B/D revealed with anti-BD. (D) Relative distribution of NBCn2-B/D, averaged from 6 blots, using the same approach as for panel B. (E) Typical western blot of NBCn2-C/D revealed with anti-CD. (F) Relative distribution of NBCn2-C/D, averaged from 6 experiments, as in panels B and D. CX: Cerebral cortex; SCX: subcortex; CB: cerebellum; HC: hippocampus; MD: medulla. For bar graphs, data are presented as means ± SE.

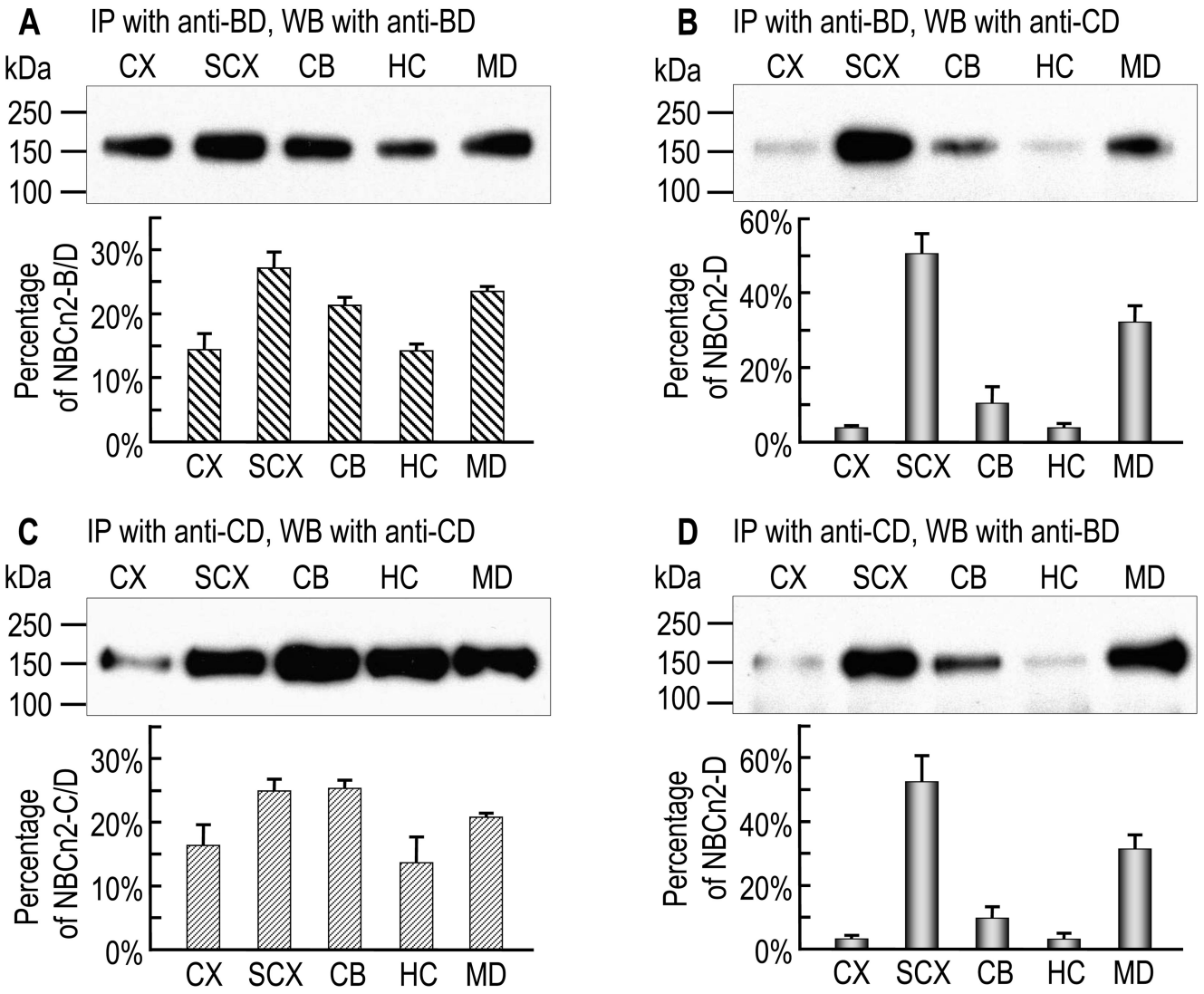

Fig. 4.

Relative distribution of NBCn2 splice variants in mouse brain regions. (A) NBCn2-B/D. Upper panel: representative blot of NBCn2-B/D. Lower panel: summary of fractional percentage of NBCn2-B/D in the five regions of mouse brain. Membrane proteins from mouse brain were immunoprecipitated with anti-BD, the blot was probed with anti-BD. (B) NBCn2-D. Upper panel: representative blot showing the distribution of NBCn2-B/D. Lower panel: summary of fractional percentage of NBCn2-B/D in the five regions of mouse brain. A parallel blot to that shown in panel A was probed with anti-CD. (C) NBCn2-C/D. Upper panel: representative blot showing the distribution of NBCn2-C/D. Lower panel: summary of fractional percentage of NBCn2-C/D in the five regions of mouse brain. Membrane proteins from mouse brain were immunoprecipitated with anti-CD, the blot was probed with anti-CD. (D) NBCn2-D. Upper panel: representative blot showing the distribution of NBCn2-D. Lower panel: summary of fractional percentage of NBCn2-D in the five regions of mouse brain. A parallel blot to that shown in panel C was probed with anti-BD. For all bar graphs, the fractional data were computed using similar approaches to that in Fig. 3B.

For all bar graphs, N=4 pools of material (each pool representing 2–4 adult mice). Data are presented as mean ± SE. IP: immunoprecipitation; WB: western blot.

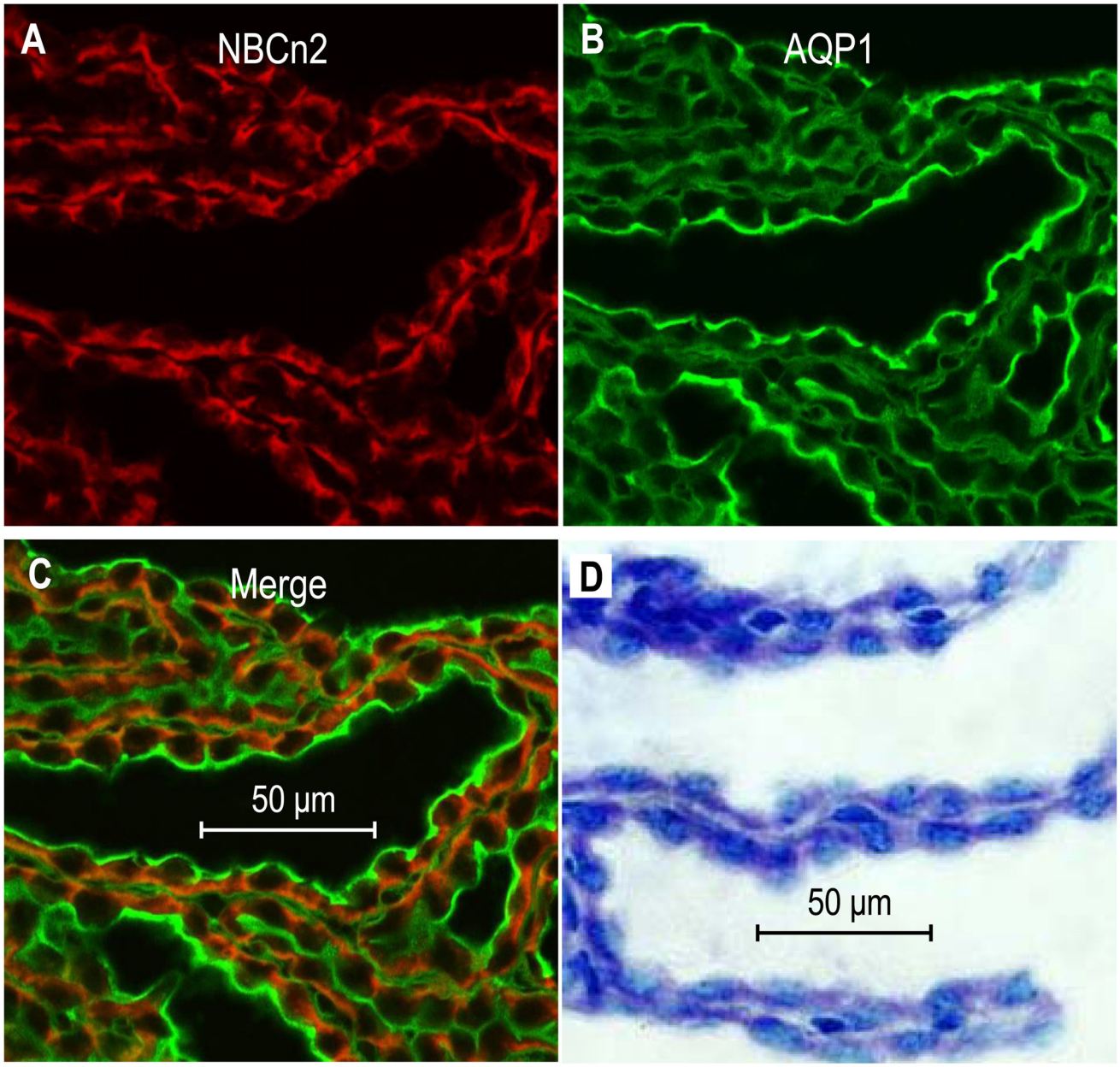

Fig. 5.

Indirect immunofluorescence of NBCn2 in the choroid plexus of the fourth ventricle of mouse brain. The sections were double-stained with affinity-purified anti-ABCD (red, panel A) and a monoclonal anti-AQP1 antibody (green, panel B). Panel C is the merge of anti-ABCD and anti-AQP1. (D) Staining of choroid plexus with thionin on an adjacent section.

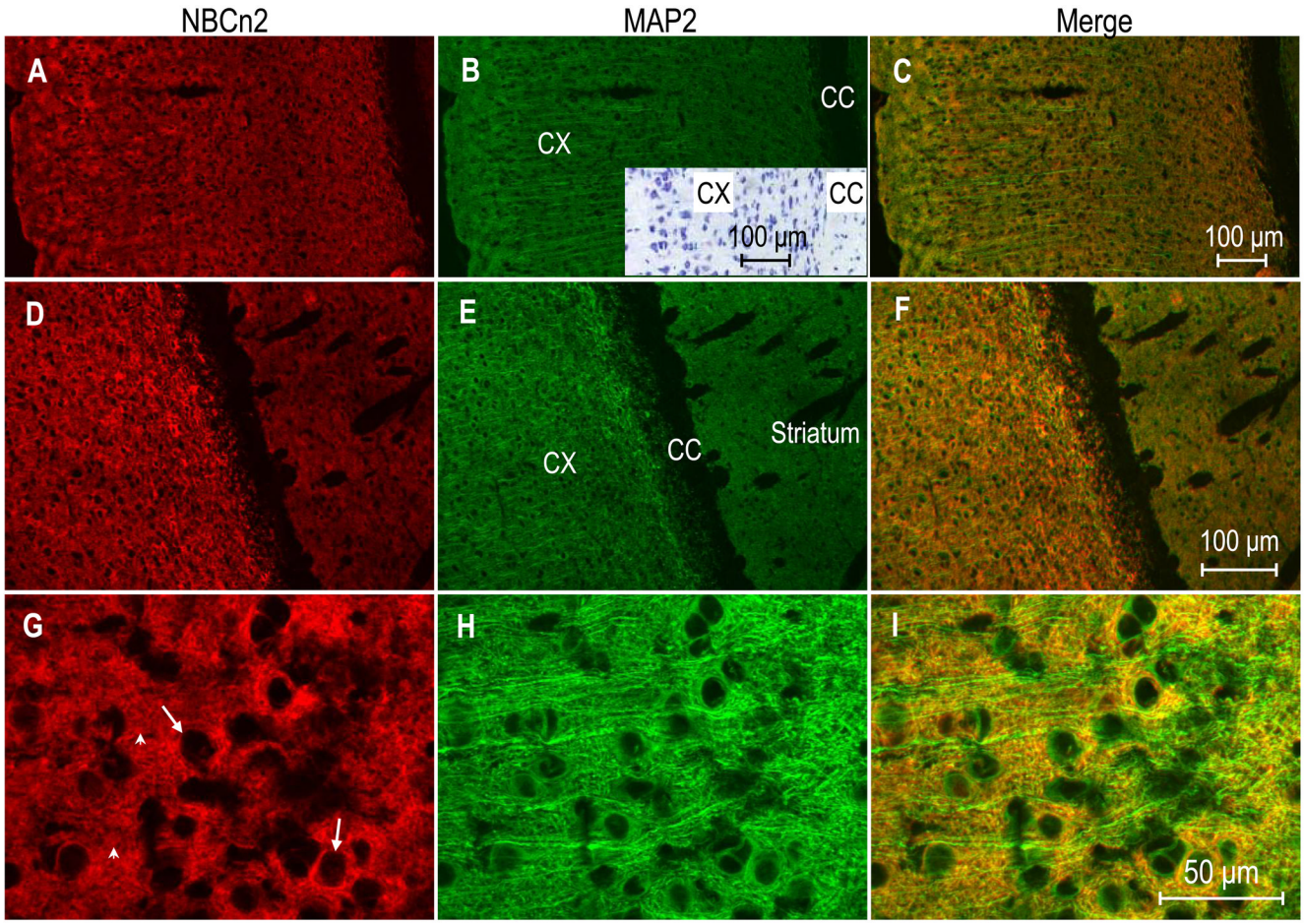

Fig. 6.

Indirect immunofluorescence of NBCn2 in the cerebrum of mouse brain. The sections were double-stained with affinity-purified anti-ABCD (red in panels A, D, G) and the neuronal marker MAP2 antibody (green in panels B, E, H). (A–C) A low-magnification view showing the expression of NBCn2 in cerebral cortex (CX). Inset in panel B: Staining of cerebral cortex with thionin on an adjacent section. (D–F) A low-magnification view showing the distribution of NBCn2 in CX, corpus callosum (CC) and striatum. (G–I) A higher-magnification view of CX, taken from a different area of the same section as in panels A–C. Each long arrow in panel D points to a region near the plasma membrane of a neuron soma. The arrow heads point to neuronal processes.

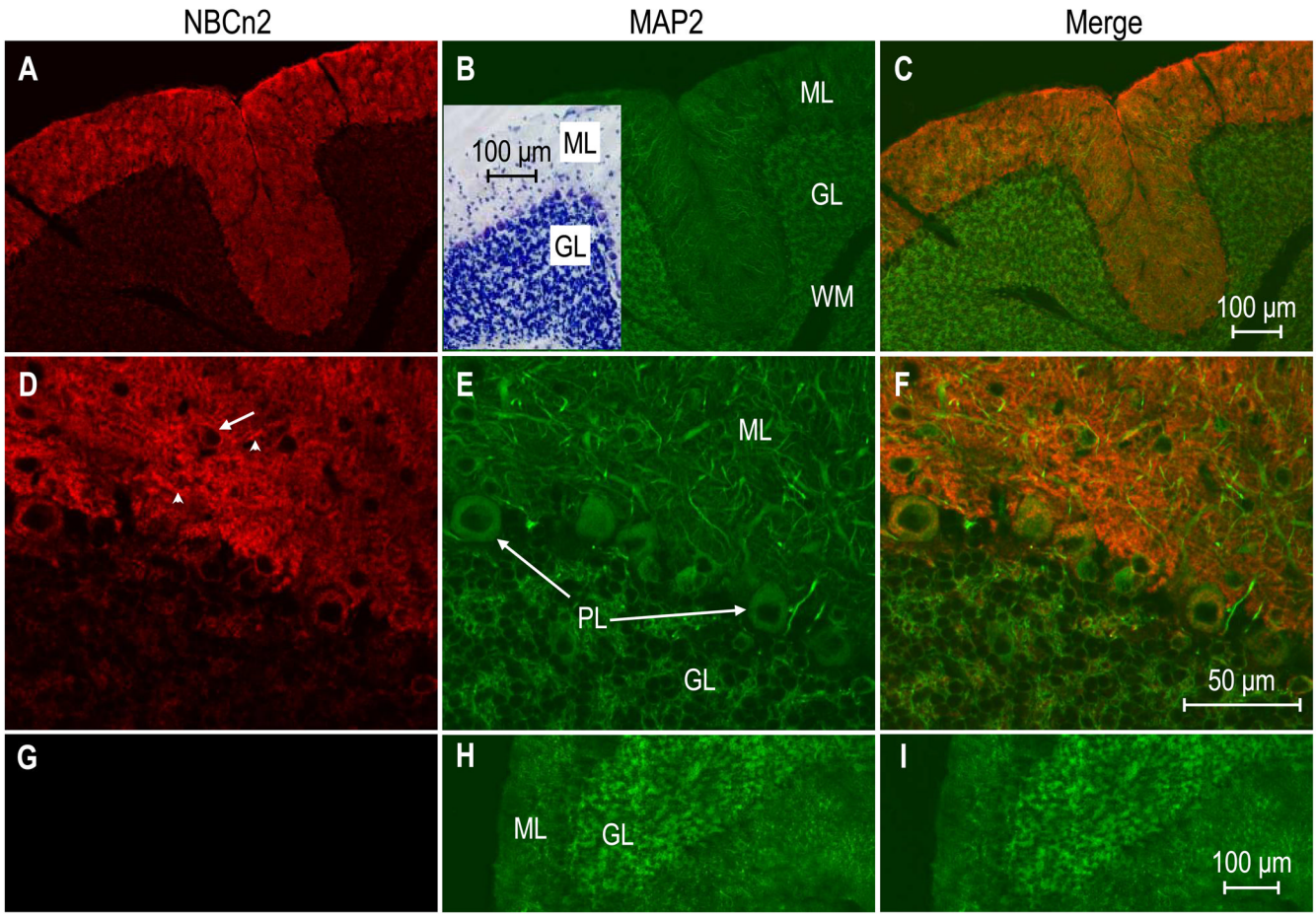

Fig. 7.

Indirect immunofluorescence of NBCn2 in mouse cerebellum sections. Sections (A–F) were double-stained with affinity-purified anti-ABCD (red in panels A, D) and the neuronal marker MAP2 antibody (green in panels B, E). (A–C) A low-magnification view showing the distribution of NBCn2 in different layers of mouse cerebellum. Inset in panel B: Staining of cerebellum with thionin on an adjacent section. (D–F) A higher-magnification view from a different area of the same section as in panels A–C. The long arrow in panel D points to a region near the plasma membrane of a neuron soma. The arrow heads point to a neuronal process. (G–I) Immunodepletion of anti-ABCD. The anti-ABCD was immunodepleted prior to immunohistochemistry staining of the section. ML: molecular layer; GL: granular layer; WM: white matter; PL: Purkinje-cell layer.

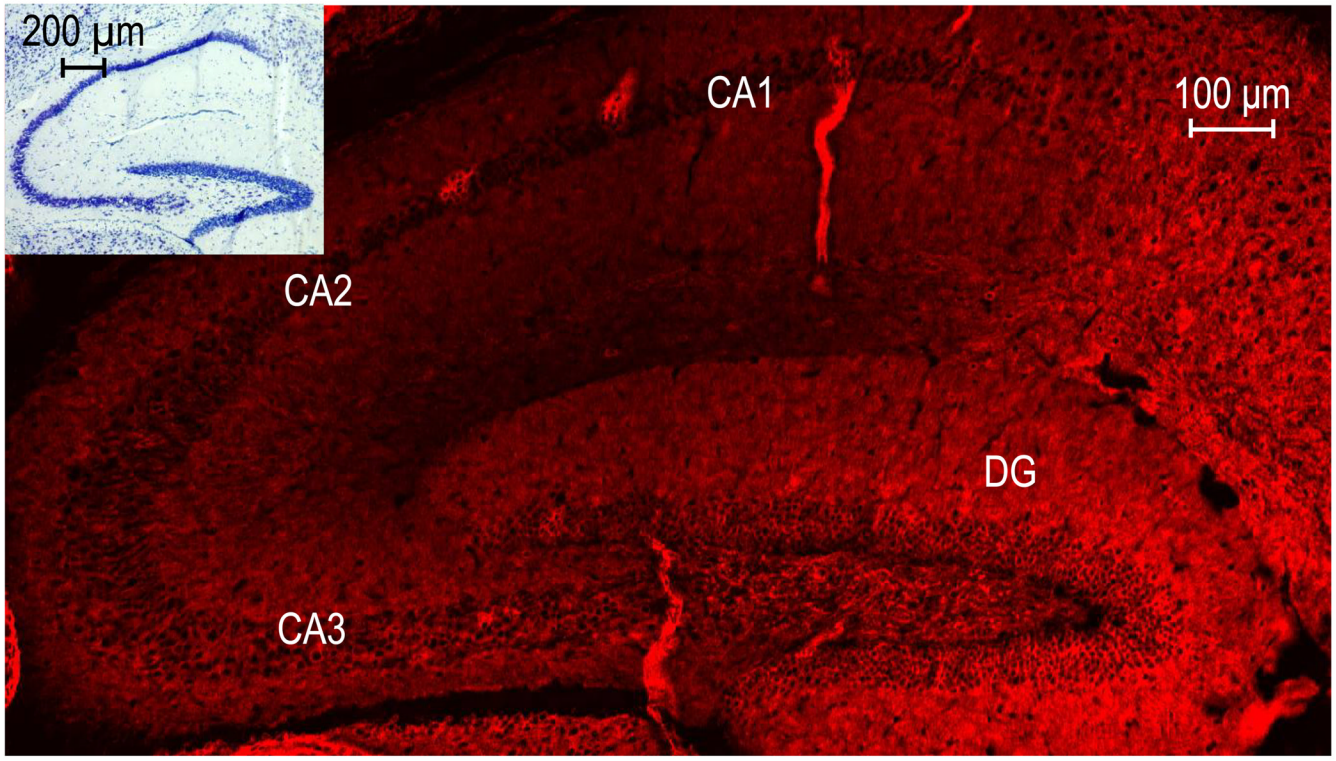

Fig. 8.

Indirect immunofluorescence of NBCn2 in mouse hippocampal section. A hippocampus section of mouse brain was stained with affinity-purified anti-ABCD. The picture was generated by aligning two images in order to show a whole view of hippocampus. Inset: Staining of hippocampus with thionin on an adjacent section.

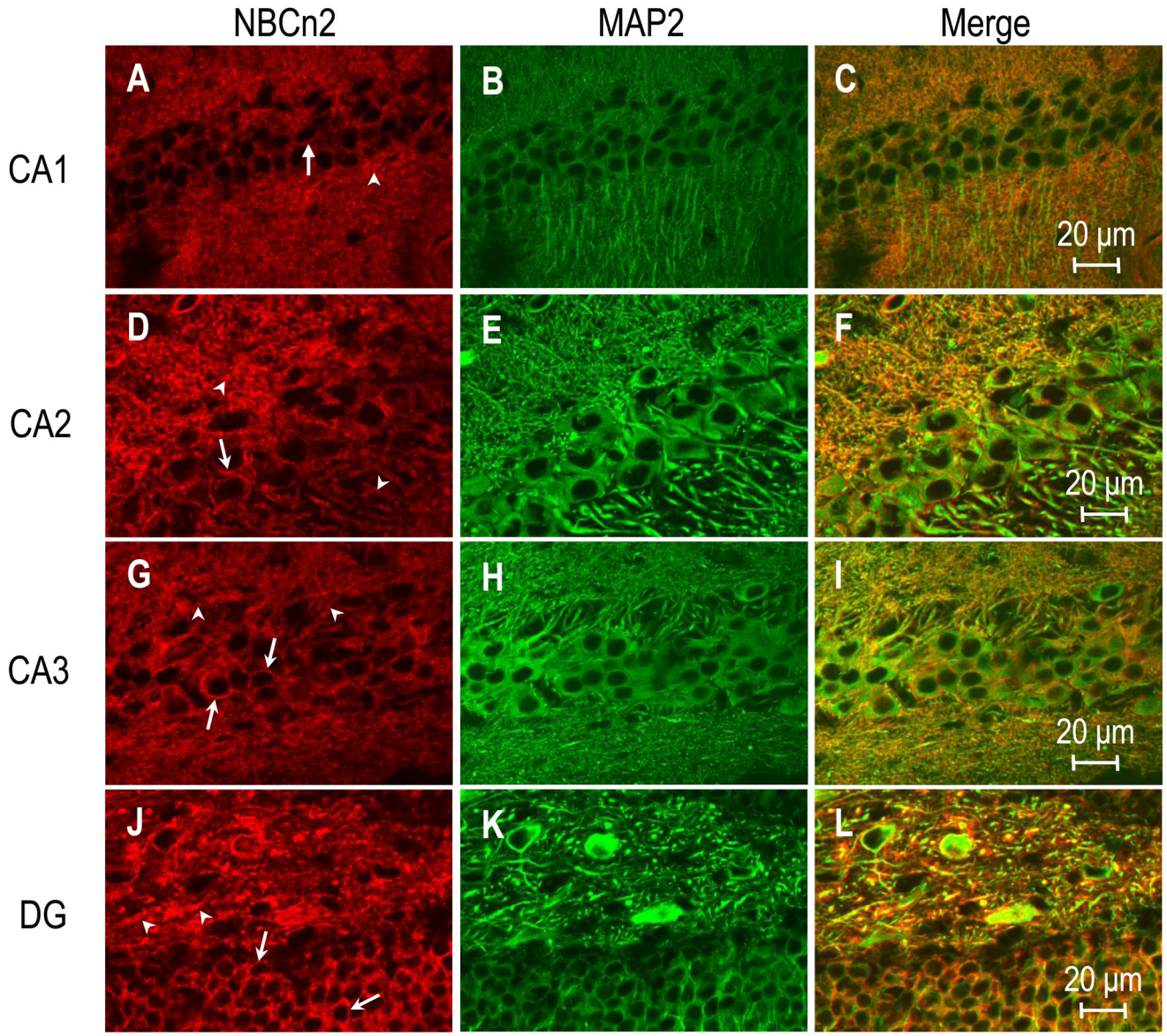

Fig. 9.

Indirect immunofluorescence of NBCn2 in mouse hippocampal section. A section of mouse hippocampus was stained with affinity-purified anti-ABCD (red in panels A, D, G, J) and neuronal marker MAP2 (green in panels B, E, H, K). (A–C) CA1. (D–F) CA2. (G–I) CA3. (J–L) dentate gyrus (DG). Each long arrow points to a region near the plasma membrane of a neuron soma. The arrow heads point to neuronal processes.

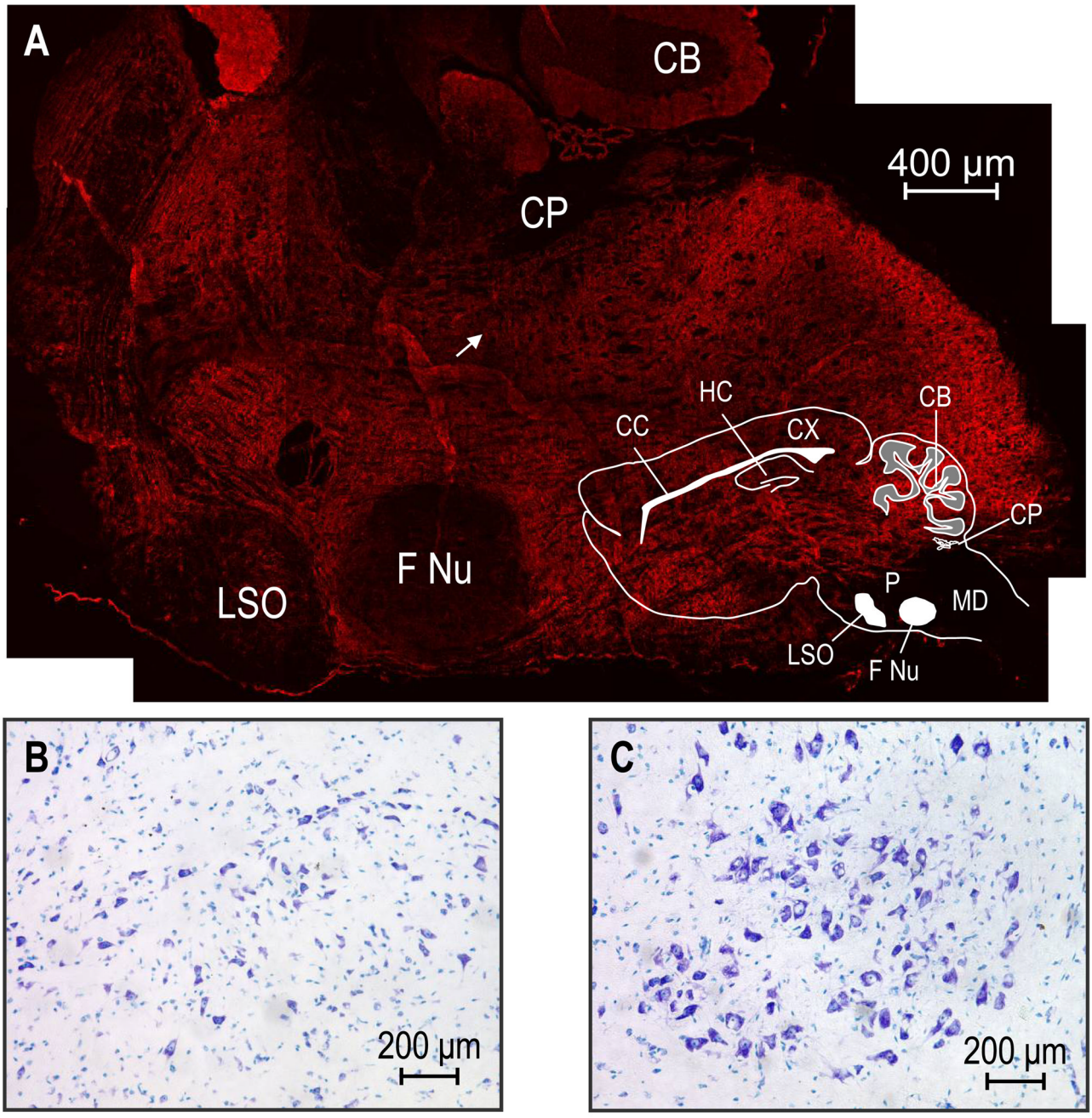

Fig. 10.

Indirect immunofluorescence of NBCn2 in a sagittal section of mouse brainstem. (A) Distribution of NBCn2 staining using affinity-purified anti-ABCD antibody. The picture was generated from 23 separated images in order to show a whole view of the medulla. (B) Thionin staining of LSO nucleus in a section adjacent to that in panel A. (C) Thionin staining of facial nucleus (F Nu) in a section adjacent to that in panel A. CB: cerebellum; CC: corpus callosum; CP: choroid plexus of the 4th ventricle; CX: cerebral cortex; HC: hippocampus; LSO: lateral superior olive; P: Pons; MD: medulla.

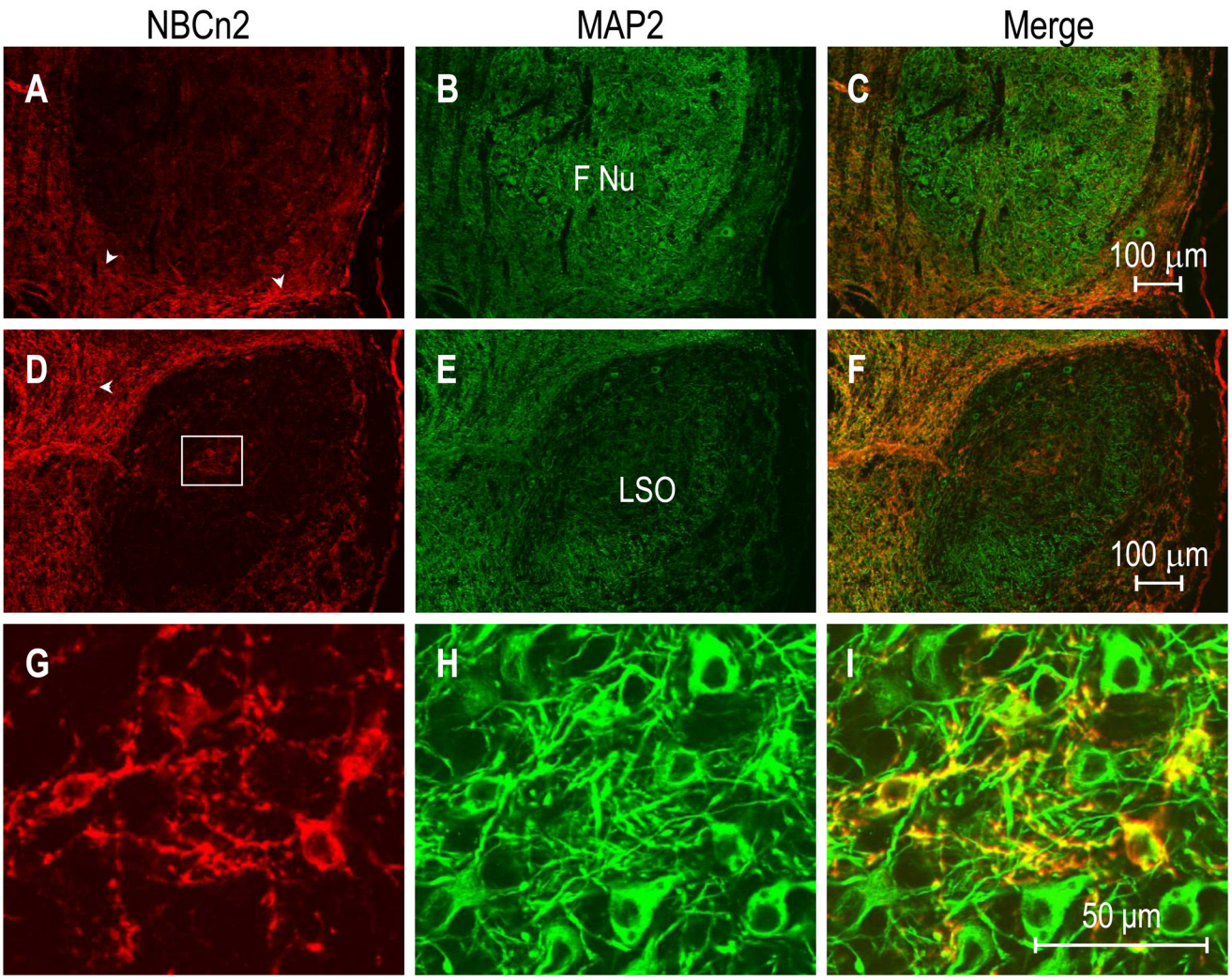

Fig. 11.

Indirect immunofluorescence of NBCn2 in sections of mouse brainstem. A section was double-stained with affinity-purified anti-ABCD (red in panels A, D, G) and the neuronal marker MAP2 antibody (green in panels B, E, H). (A–C) A low-magnification view of facial nucleus (F Nu). (D–F) A low-magnification view of lateral superior olive (LSO). Arrowheads in A and D indicated NBCn2 expression in area surrounding the nuclei. (G–I) A higher-magnification view of the region surrounded by the rectangle in panel D of the central LSO.

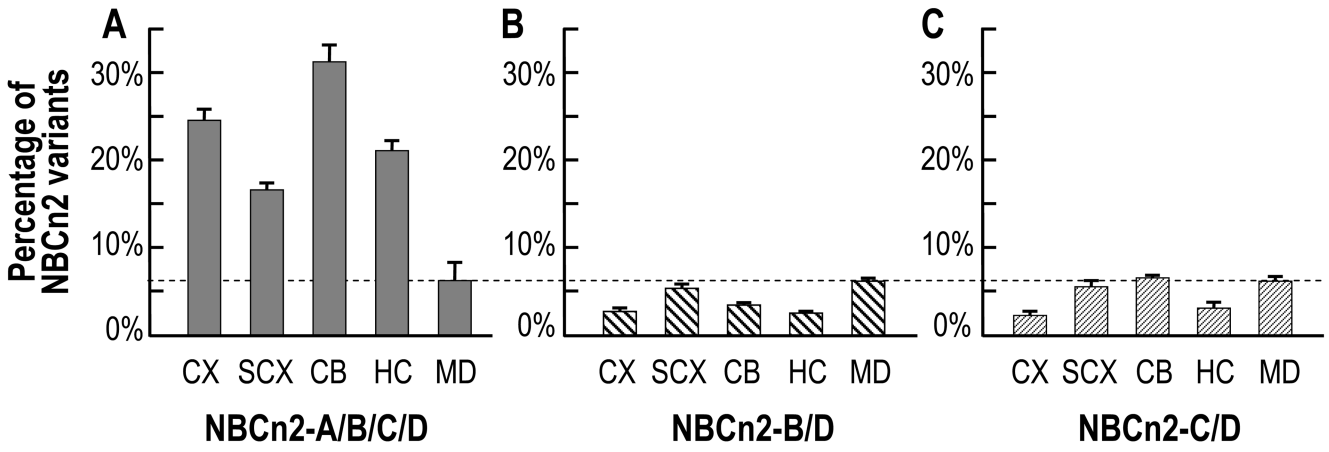

Fig. 12.

Fractional contribution of NBCn2-A/B/C/D, NBCn2-B/D, and NBCn2-C/D to the total NBCn2 protein in mouse brain. Panel A is a replot of Fig. 3B. We created panel B from Fig. 3D by assuming that no NBCn2-A or -C is expressed in MD, and thus that all NBCn2 in MD is NBCn2-B/D. We then rescaled Fig. 3D so that the MD bar in panel B has the same height as the MD bar in panel A. Thus, the distribution in panel B is an estimate of the contribution of NBCn2-B/D to total NBCn2 protein in the five mouse brain regions. Similarly, we created panel C from Fig. 3F by assuming that no NBCn2-A or -B is expressed in MD, and thus that all NBCn2 in MD is NBCn2-C/D. We then rescaled Fig. 3F so that the MD bar in panel C has the same height as the MD bar in panel A. Thus, the distribution in panel C is an estimate of the distribution of NBCn2-C/D to total NBCn2 protein in the five mouse brain regions.

Table 1

Sequence of peptides used for antibody generation

Antibody	Peptide for immunizing rabbit	Accession#	Note
Anti-ABCD	MEIKDQGAQMEPLLPTRNC*	BAB18301	First 18 aa of NBCn2 Nt
Anti-BD	CGMKQRLDKGPPHQQERE	AAQ59640	18 aa in cassette A of NBCn2-B/D
Anti-CD	SIESRKEKKADSGKGVDRETCLC*	AAO59639	Unique Ct of NBCn2-C/D

*C-terminal cysteine was added for conjugation to keyhole limpet hemocyanin.

Table 2

Estimation of fractional distribution of NBCn2 variants in mouse brain regions

% in total NBCn2	CX	SCX	CB	HC	MD	Total
ABCD	25%	17%	31%	21%	6%	100%
BD	4%	5%	3%	3%	6%	21%
CD	2%	6%	7%	3%	6%	24%
Thus, A	>19%	>6%	>21%	>15%	−6%	>55%